Chemical Science

EDGE ARTICLE

View Article Online
View Journal

Cite this: DOI: 10.1039/c4sc01731e

Base catalytic activity of alkaline earth MOFs: a (micro)spectroscopic study of active site formation by the controlled transformation of structural anions†

P. Valvekens,[a] D. Jonckheere,[a] T. De Baerdemaeker,[a] A. V. Kubarev,[a] M. Vandichel,[b] K. Hemelsoet,[b] M. Waroquier,[b] V. Van Speybroeck,[b] E. Smolders,[c] D. Depla,[d] M. B. J. Roeffaers[a] and D. De Vos*[a]

Received 11th June 2014
Accepted 25th July 2014

DOI: 10.1039/c4sc01731e

www.rsc.org/chemicalscience

A new method has been developed for generating highly dispersed base sites on metal–organic framework (MOF) lattices. The base catalytic activity of two alkaline earth MOFs, $M_2(BTC)(NO_3)(DMF)$ (M = Ba or Sr, H_3BTC = 1,3,5-benzenetricarboxylic acid, DMF = *N*,*N*-dimethylformamide) was studied as a function of their activation procedures. The catalytic activity in Knoevenagel condensation and Michael addition reactions was found to increase strongly with activation temperature. Physicochemical characterization using FTIR, ^{13}C CP MAS NMR, PXRD, XPS, TGA-MS, SEM, EPR, N_2 physisorption and nitrate content analysis shows that during activation, up to 85% of the nitrate anions are selectively removed from the structure and replaced with other charge compensating anions such as O^{2-}. The defect sites generated *via* this activation act as new strong basic sites within the catalyst structure. A fluorescence microscopic visualization of the activity convincingly proves that it is exclusively associated with the hexagonal crystals, and that reaction proceeds inside the crystal's interior. Theoretical analysis of the Ba-material shows that the basicity of the proposed Ba^{2+}–O^{2-}–Ba^{2+} motifs is close to that of the edge sites in BaO.

Introduction

Metal–organic frameworks (MOFs) have attracted much interest due to their high compositional and structural diversity. Numerous applications have been investigated so far, such as gas storage, separation and catalysis.[1–3] The exploration of MOFs as catalysts, however, has mainly focused on acid or redox catalysis. Reports on the catalytic activity of MOFs in base-catalyzed reactions are much more scarce, mainly focusing on porous materials containing N-functionalized linkers, *e.g.* aminoterephthalic acid.[4–7] In these materials, the N-functionality acts as the basic catalytic site. However, the relatively weak basicity of these sites, which have electron-withdrawing carboxylic groups on the same aromatic ring, limits the reaction scope of these catalysts. Furthermore, a recent study has shown that the catalytic activity of the amino-substituted Zn-MOF IRMOF-3 can be attributed to defect sites rather than to the amine functionality.[8] A second, smaller group of basic MOF catalysts comprises structures without micropores or with very narrow micropores, featuring basic sites mainly at lattice terminating surface sites. Examples of such materials include ZIF-8 and ZIF-9,[9–11] in which the pore windows are too narrow to allow the diffusion of most reactants and/or products, and a Ba-3,5-pyrazoledicarboxylate MOF which has a limited microporous volume.[12] If catalysis is confined to the outer surface, only a very limited fraction of the catalytic material is used, and the precise nature of the sites at the surface is not always well defined.

Rather than focusing on the linker as a source of basic sites, modification of the inorganic building unit is an alternative option for creating basicity in MOFs. Metal oxides such as MgO, CaO, SrO and BaO are generally known to be active, industrially applied basic catalysts.[13,14] This activity is attributed to low-coordination sites located on the crystal surface or at corners and edges.[15,16] The high dispersion of metal–oxygen or metal–hydroxide strands, for example, in certain alkaline earth metal MOFs may provide a starting point for imparting base catalytic activity to these MOFs. The challenge is then to develop

[a]*Centre for Surface Chemistry and Catalysis, KU Leuven – University of Leuven, Kasteelpark Arenberg 23, box 2461, 3001 Leuven, Belgium. E-mail: dirk.devos@biw.kuleuven.be*

[b]*Center for Molecular Modeling, Universiteit Gent, Technologiepark 903, 9052 Zwijnaarde, Belgium*

[c]*Department of Earth and Environmental Sciences, KU Leuven – University of Leuven, Kasteelpark Arenberg 20, 3001 Leuven, Belgium*

[d]*Department of Solid State Chemistry, Universiteit Gent, Krijgslaan 281 S1, 9000 Ghent, Belgium*

† Electronic supplementary information (ESI) available: Additional figures, experimental procedures, catalytic data on other alkaline earth metal MOFs, mass spectra of reaction products, details on the theoretical modelling. See DOI: 10.1039/c4sc01731e

activation procedures to generate uniform, localized defects throughout the structure without causing complete structural decay. With such an aim, the present study focuses on active site formation in the Ba- and Sr-MOFs $M_2(BTC)(NO_3)(DMF)$ (M = Ba or Sr, H_3BTC = 1,3,5-benzenetricarboxylic acid, DMF = *N*,*N*-dimethylformamide). These structures were first reported by Foo *et al.*[17] and Lee *et al.*[18] for the Ba- and the Sr-variants, respectively, and exhibit some remarkable structural features. The connectivity of the inorganic building units in most MOFs is of a 0, 1 or 2-dimensional nature, forming inorganic nodes, chains or planes; however, the M–O–M bonds in these Ba- and Sr-materials extend in 3 dimensions. Such frameworks can therefore be classified as I^3O^0 type frameworks, according to Cheetham *et al.*[19] The inorganic building units and the trimesate linkers combine to form hexagonal prism shaped crystals with large three-leaf-clover-shaped channels running along the length of the crystals in the [001] direction (Fig. 1, top). The pore dimension of each channel is approximately 13 Å at its widest point and 6.5 Å at its narrowest part. Most important in this study, however, is the presence of nitrate anions in the structure. These anions line the walls of the pores and are required for charge neutrality (Fig. 1, bottom). Here we show that thermal pretreatment of these materials results in the controlled decomposition of the nitrate anions, along with the formation of Ba^{2+}–O^{2-}–Ba^{2+} motifs along the channels. These provide the material with a high level of activity in base-catalyzed reactions. Fluorescence microscopy proves that the activity is situated inside the channels of the MOF.

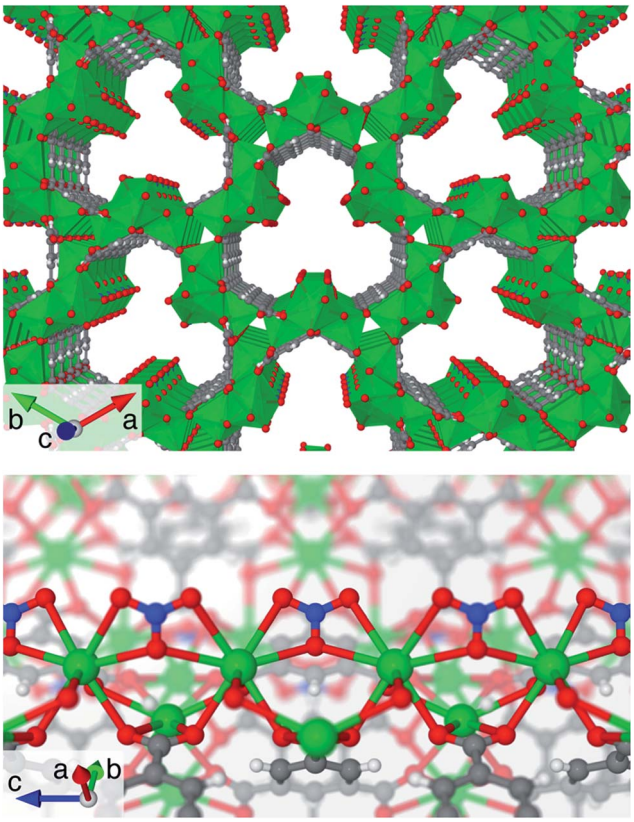

Fig. 1 Pore structure of $Ba_2(BTC)(NO_3)$ (top) and close-up of the nitrate chain running lengthwise through the pores of the MOF (bottom). Green, blue, red, grey and white represent barium, nitrogen, oxygen, carbon and hydrogen respectively.

Results and discussion

Catalytic activity of the $Ba_2(BTC)(NO_3)$ and $Sr_2(BTC)(NO_3)$ derived materials

As the interests of the MOF community have often focused on sorption applications, the creation of permanent porosity by pore evacuation has been studied in detail for many materials. A highly evacuated state, however, does not necessarily correspond to the most catalytically active state of a material; hence, the activation procedures for the Ba- and Sr-MOFs were optimized with regard to the catalytic activity rather than aiming for the largest values for pore volume. The catalytic activities of the Ba- and Sr-MOFs, activated at different temperatures, were evaluated using model Knoevenagel condensation and Michael addition reactions at 70 °C (Scheme 1). Besides the $Ba_2(BTC)(NO_3)$ and $Sr_2(BTC)(NO_3)$ MOFs, a range of other alkaline earth dicarboxylate MOFs were included in a preliminary activity screening (see ESI†). These activation treatments did not result in any increase in activity for most of the materials studied; however, for $Ba_2(BTC)(NO_3)$, an elevated activation temperature was found to produce a remarkably large increase in its catalytic activity for the different reactions (Fig. 2). For instance, with $Ba_2(BTC)(NO_3)$ pretreated at 320 °C as the catalyst, the Knoevenagel condensation of malonitrile and benzaldehyde, or the Michael addition of ethyl cyanoacetate to methyl vinyl ketone, proceeded with yields of 99% and 93%, respectively. A similar effect was found for the isostructural Sr-MOF (Fig. 2 inset). In general, the activity of the $Sr_2(BTC)(NO_3)$ MOF after activation at 320 °C was somewhat lower than that of the related Ba-material; as illustrated, for instance, by the Knoevenagel condensation reaction of ethyl cyanoacetate (ECA) and benzaldehyde. For alkaline earth metal oxides, basic strength is known to decrease in the order BaO > SrO > CaO > MgO.[20] The similarity of the order of activity for the activated Ba- *vs.* Sr-MOFs already suggests that alkaline earth ions are intimately involved in the base catalytic activity.

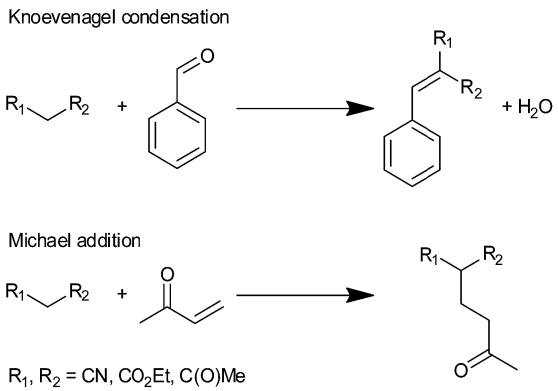

Scheme 1 Schematic representations of the model Knoevagel condensation and Michael addition reactions.

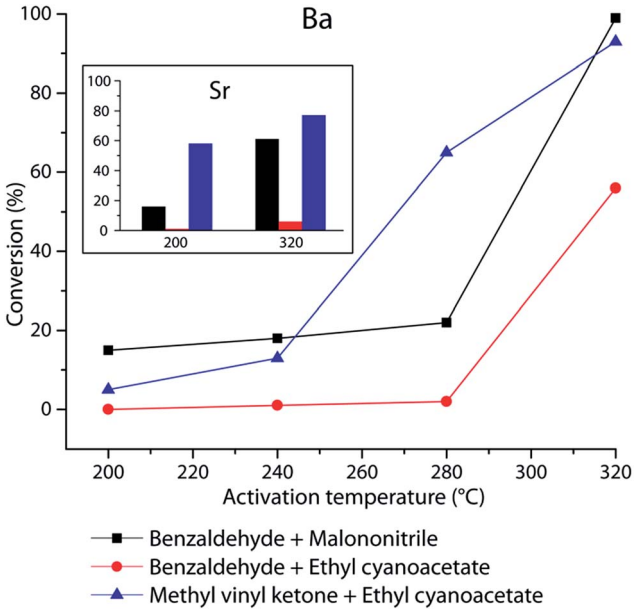

Fig. 2 Conversion of acceptor molecules observed after a 24 h reaction time at 70 °C for Knoevenagel condensation and Michael addition reactions, as a function of the activation temperature for the Ba-MOF and the Sr-MOF (inset).

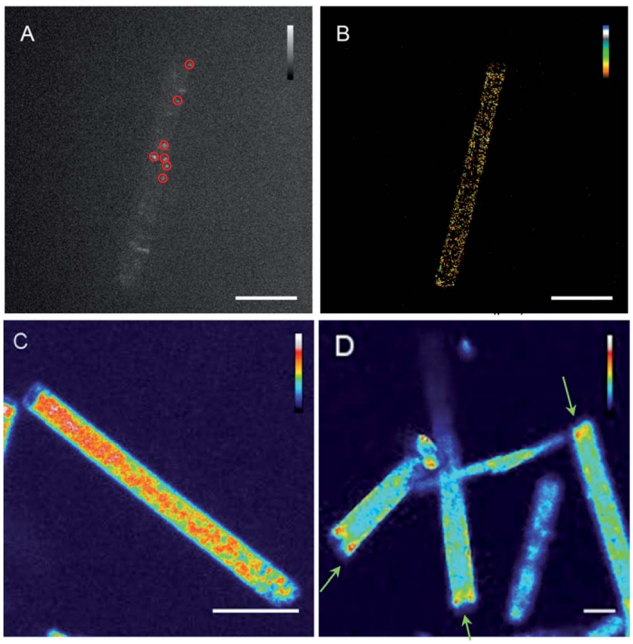

Fig. 3 Fluorescence microscopy of $Ba_2(BTC)(NO_3)$. (A) Wide-field FM image of fluorescein diacetate (FDA; 4.2×10^{-7} M) conversion (red circles indicate localized single reaction events); (B), NASCA reactivity map generated by the localization of reaction events during 150 seconds; (C) confocal FM image of the FDA (1×10^{-4} M) conversion; (D) confocal FM image of the onset of fluorescence soon after the introduction of FDA. Green arrows indicate the local increase in fluorescence in the tips of the crystal. Scale bars for all images are 5 μm.

The reactivity of different donor molecules was investigated using $Ba_2(BTC)(NO_3)$ activated overnight at 320 °C as a standard catalyst. Besides malononitrile and ethyl cyanoacetate, ethyl acetoacetate was also used for Knoevenagel condensation with benzaldehyde (Table 1, entries 1–3). Although the reaction temperature was increased from 70 °C to 110 °C, only a limited conversion of ethyl acetoacetate was observed after 24 h, compared to the reactions of the more acidic malononitrile or ethyl cyanoacetate donors. This clearly shows that, at least for the Knoevenagel condensation reaction, the acidity of the donor molecule strongly determines the overall conversion, as is expected for a base-catalyzed reaction. When malononitrile is used as the donor molecule, the benzaldehyde acceptor molecule can be readily replaced by its functionalized variants, *e.g.* *p*-bromo- or *p*-nitrobenzaldehyde, without a significant loss in conversion (entries 4–7). Acetophenone as an acceptor molecule leads to diminished yield, probably due to steric hindrance (entry 8), whereas the cyclic ketones cyclopentanone

Table 1 Exploration of the substrate scope of the $Ba_2(BTC)(NO_3)$ material activated at 320 °C for 16 h[a]

	Donor	pK_a (DMSO)	Acceptor	$X_{acceptor}$,%
1	Malononitrile	11.1	Benzaldehyde	97
2	Ethyl cyanoacetate	13.1	Benzaldehyde	85
3	Ethyl acetoacetate	14.3	Benzaldehyde	6
4	Malononitrile	11.1	*p*-Bromobenzaldehyde	92
5	Malononitrile	11.1	*p*-Nitrobenzaldehyde	88
6	Malononitrile	11.1	*o*-Nitrobenzaldehyde	80
7	Malononitrile	11.1	*p*-Methoxybenzaldehyde	72
8	Malononitrile	11.1	Acetophenone	3
9	Malononitrile	11.1	Cyclopentanone	29
10	Malononitrile	11.1	Cyclohexanone	92
11	Malononitrile	11.1	Methyl vinyl ketone	33
12	Ethyl cyanoacetate	13.1	Methyl vinyl ketone	77
13	2,4-Pentanedione	13.3	Methyl vinyl ketone	99
14	Ethyl acetoacetate	14.3	Methyl vinyl ketone	99
15	Diethyl malonate	16.4	Methyl vinyl ketone	1

[a] Reaction conditions: 1 mmol of each reactant; 2 ml toluene, 110 °C, 50 mg MOF.

and cyclohexanone show moderate to high conversions (entries 9–10).

For the Michael addition reactions (Table 1, entries 11–15), the correlation between the acidity of the donor molecule and the overall conversion is less straightforward. Even with moderately acidic donors like 2,4-pentanedione or ethyl acetoacetate, excellent conversions are achieved (99%; entries 13–14), while conversion of a more acidic reactant like malononitrile is somewhat lower (entry 11). The fact that the rates are not solely dependent on the acidity of the donor suggests that in the Michael addition reaction, the $Ba_2(BTC)(NO_3)$ catalyst activates not only the donor molecules, but also the acceptor molecules. Specifically, the α,β-unsaturated carbonyl moiety of methyl vinyl ketone could be activated on the Lewis acid component of the acid-base pair of the active site.[21] The limited conversion for the reaction of diethyl malonate (entry 15), however, illustrates that too low a pK_a may still adversely affect the overall conversion for a Michael donor that lacks nitrile functionalities.

Fluorescence microscopy was used to confirm the base catalytic activity of the MOF material (Fig. 3). NASCA (Nanometer Accuracy by Stochastic Chemical Reaction) microscopy records the individual catalytic conversions of a non-fluorescent reactant molecule to a strongly fluorescent product molecule; fluorescein diacetate (FDA) and fluorescein, respectively, were used in this study.[22] There are two major observations: first, that the catalytic activity is clearly associated with the hexagonal prism-shaped MOF crystals, and not with debris or disintegrated crystals. Secondly, a homogeneous activity level was observed throughout the whole crystal. To better confirm the occurrence of catalytic activity in the center of the MOF particles, confocal imaging with the focal plane located at the center of the crystals was performed. These measurements reveal that transesterification, even of the bulky FDA probe molecules, occurs over the entire volume of the catalyst particle. Moreover, when the onset of fluorescence was monitored by confocal microscopy directly after the addition of FDA, a gradient in fluorescence could be observed along the long axis of the crystals, corresponding to the channels in the [001] direction. As expected, this gradient is due to the gradual diffusion of FDA in the pores. Active sites located near the pore openings are more easily reached by the FDA and display greater catalytic activity, reflected in a stronger fluorescence than the active sites located near the center of the hexagonal crystals.

Finally, the heterogeneity of the $Ba_2(BTC)(NO_3)$ catalyst activated overnight at 320 °C was evaluated *via* a hot filtration test, which was performed on a Michael addition reaction of ethyl cyanoacetate and methyl vinyl ketone in toluene at 70 °C (Fig. S1, ESI†). Removal of the catalyst after a 2 h reaction time confirmed that catalysis is indeed fully heterogeneous. Repeated use of the $Ba_2(BTC)(NO_3)$ catalyst in consecutive runs of the Knoevenagel condensation of benzaldehyde and malononitrile showed that the catalyst is reusable (Fig. S2†). The catalyst maintained its high activity (99% conversion after 24 h) in the same reaction after contact with air followed by a mild drying procedure, illustrating that it is not very sensitive towards CO_2.

Elucidating the effects of the activation procedure

The activity of the tested $Ba_2(BTC)(NO_3)$ and $Sr_2(BTC)(NO_3)$ materials (as shown in Fig. 2) indicates the great influence of the activation procedure on the catalytic activity. As the largest activity increase was observed for the samples activated at 320 °C, this procedure was chosen as a standard for investigating the structural and chemical origins of the increased catalytic activity.

The removal of residual DMF molecules and other species during activation of the catalyst was monitored in a TGA-MS experiment. To fully simulate the activation procedure, TGA of $Ba_2(BTC)(NO_3)$ was performed under a He-atmosphere; the temperature profile was identical to that of the activation procedure. Three distinct transitions can be observed in the evolution of the ion count with time (Fig. 4). In the first two steps, physisorbed and chemisorbed DMF (73 Da) molecules are released from the framework. At this stage, the rise in intensity of the other mass fragments (30, 44 and 46 Da) is due to further fragmentation of DMF in the mass spectrometer. However, in the third step, centered at 300 °C, a rise in intensity can be observed for the lighter fragments (30, 44 and 46 Da), but not at all for the 73 Da signal. Hence, these signals correspond to other species than DMF. Given their mass, these are likely to be NO_x species such as NO, NO_2 and N_2O, produced by decomposition of the nitrate anions which line the pores of the material.

The loss of nitrate anions from the structure may also be observed *via* spectroscopic techniques such as FTIR and XPS spectroscopy (Fig. 5A and B, respectively). The evolution of the IR absorbance band of nitrate was monitored *in situ* during activation using a temperature- and pressure-controlled measuring cell. A loss in absorbance at 822 cm^{-1} was observed with an increasing activation time. Pure $Ba(NO_3)_2$ salt exhibits an absorbance band at 817 cm^{-1}.[23] By exchanging the DMF solvent coordinated in the pores for MeOH, the presence of this absorbance band was found to be independent from the coordinating solvent; therefore, it can be unambiguously attributed to the nitrate anions. In the XPS spectra, the N1s signal of nitrate can be found at 407 eV. Upon comparison of the signal intensities of the pristine and activated materials, using the Ba3d signal at 779 eV as an internal standard, a very substantial loss of nitrate of at least 70% was observed.

Finally, the loss of nitrate anions was unambiguously proven by measuring the nitrate and metal contents of the materials before and after activation. The nitrate content of the material could be accurately determined after dissolution of the material using a colorimetric assay, whereas the metal content was measured from the solution using ICP-MS. Prior to activation, the experimental NO_3 : Ba ratio was 0.57, which agrees rather well with the theoretically expected ratio of 0.5. After activation however, the NO_3 : Ba ratio dropped to 0.08, corresponding to a loss in nitrate content of approximately 85%. Such thermally induced decomposition of Ba-associated nitrate is actually well known, and is used in practice *e.g.* in NO_x Storage and Reduction (NSR) systems for the reduction of NO_x-emissions from lean-burn power sources.[24] Although the full mechanism is

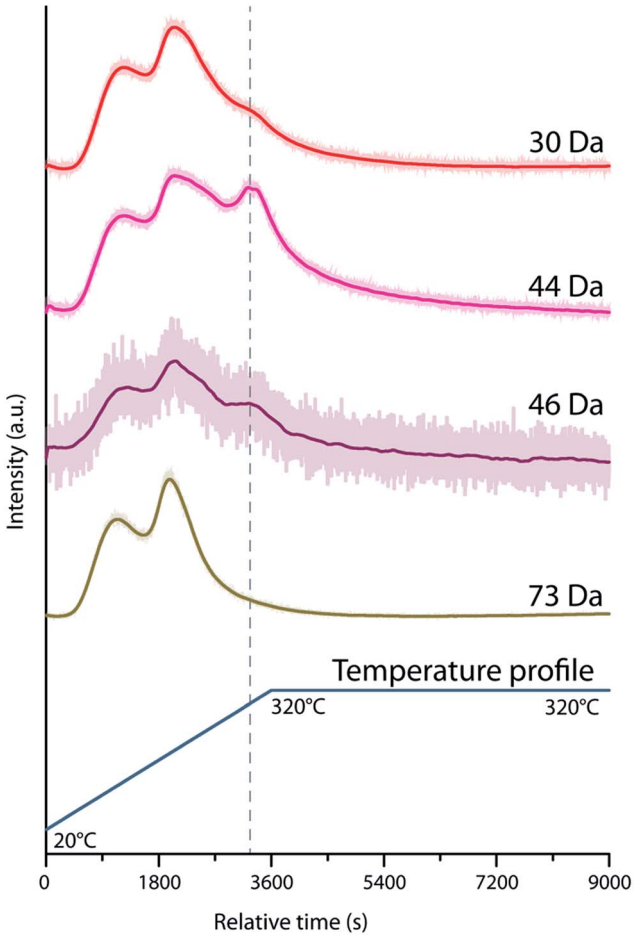

Fig. 4 Time-dependent evolution of different mass fragments in gases produced by the thermal activation of $Ba_2(BTC)(NO_3)(DMF)$, as observed *via* TGA-MS. The event at 300 °C corresponds to the decomposition of structure-embedded nitrate.

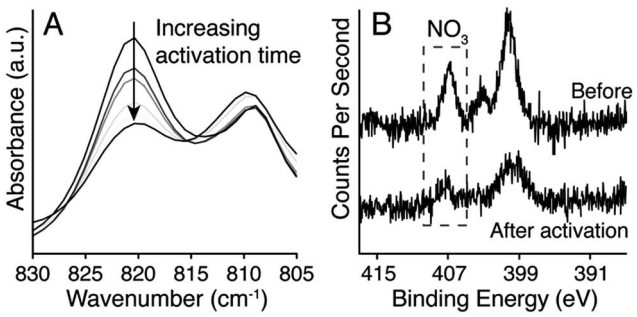

Fig. 5 Evolution of the FTIR (A) and XPS spectra (B) of the nitrate species upon activation of $Ba_2(BTC)(NO_3)$.

complex, NO_x is reversibly stored and released on BaO in these systems, according to equilibrium reactions such as:

$$BaO + 2NO_2 + 1/2O_2 \rightleftharpoons Ba(NO_3)_2$$

Both temperature and (partial) pressure are important driving forces for the conversion of nitrates back to oxides.

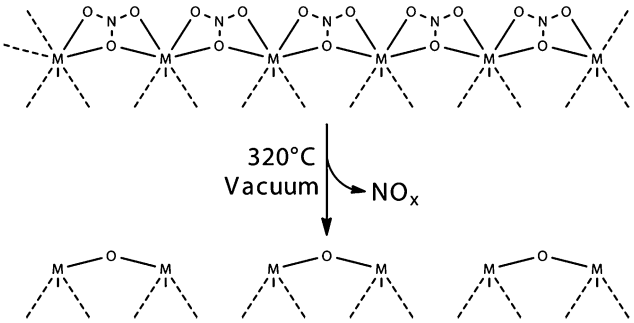

Scheme 2 Schematic representation of active site formation upon the activation of $M_2(BTC)(NO_3)$.

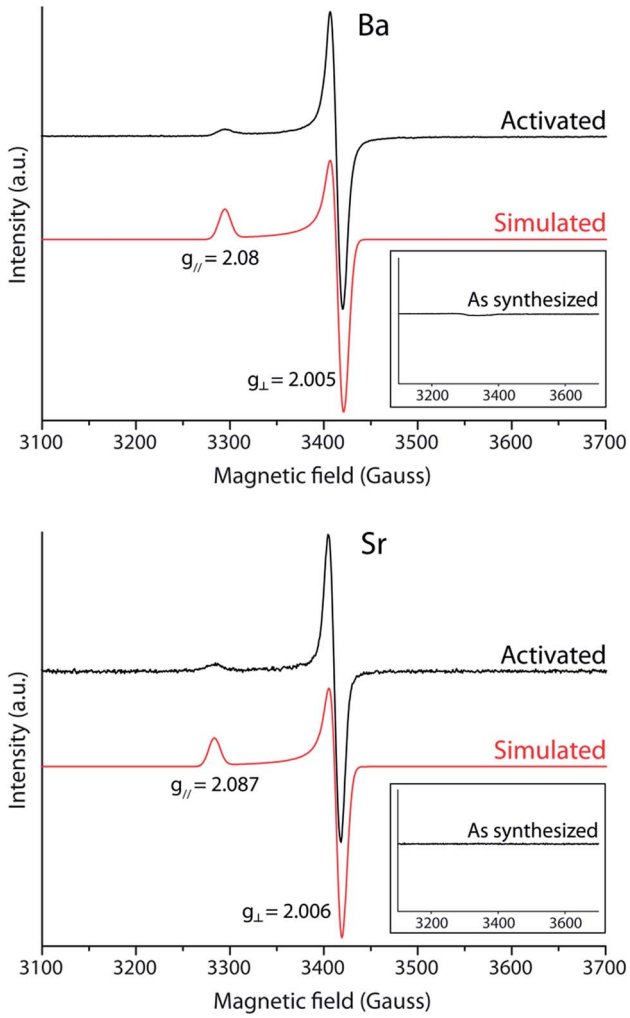

Fig. 6 EPR spectra of the Ba (above) and Sr (below) $M_2(BTC)(NO_3)$ after 16 h activation at 320 °C, compared with the simulated spectra. Inset: spectra of the samples before activation.

Increasing the temperature, as well as reducing the partial pressure of oxygen, dramatically reduces the stability of the nitrate species. Furthermore, the decomposition of barium nitrate under vacuum is reported to occur at temperatures as low as 200 °C.[25] Hence, the perfect match between the available

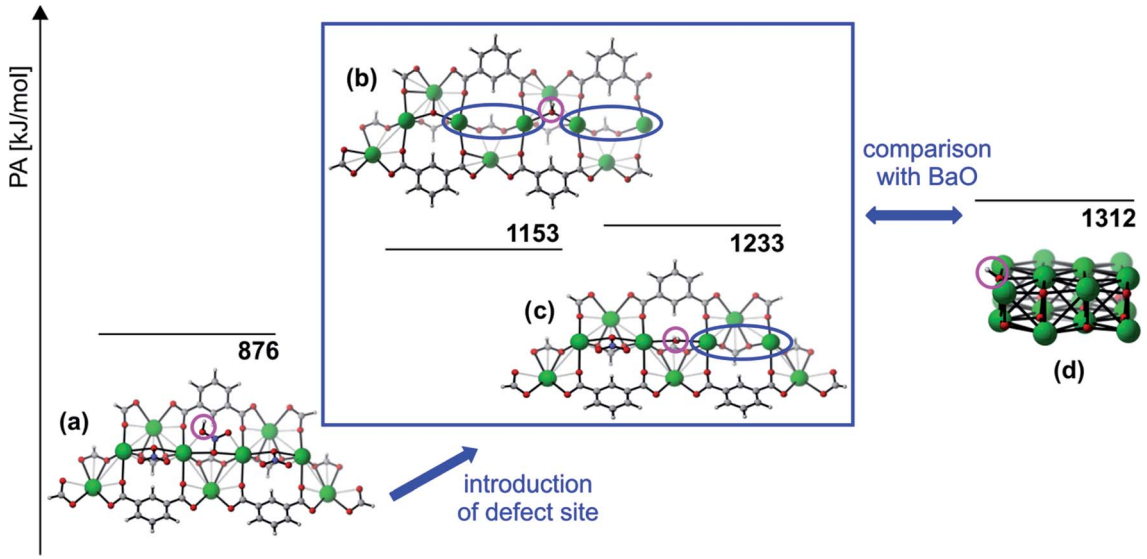

Fig. 7 Theoretical proton affinities of the optimized Ba-MOF clusters: (a) the original cluster containing NO_3 units, (b) a cluster representing a defect site and (c) a cluster containing a defect site as well as a NO_3 unit. The computed PA value of an optimized $(BaO)_{16}$ cluster (d) is also included. Values are in kJ mol^{-1} and are calculated using B3LYP/6-311G(d,p) and def2-tzvp (see computational methods). Protonated structures are depicted; the position of the proton is indicated with a purple circle and the position of the defect site is indicated with a blue circle.

literature data on $Ba(NO_3)_2$ decomposition and the observation of the gaseous decomposition products during TGA-MS on $Ba_2(BTC)(NO_3)$, strongly suggests the transformation of two MOF-embedded nitrate anions into one, surface-bound O^{2-}–anion.

The chemical stability of the linker molecules in the MOF when exposed to the activation procedure was evaluated using solid state ^{13}C CP MAS NMR (Fig. S3†). As the activation time increased, the removal of DMF molecules from the framework was apparent from the loss in intensity of the signals at 31, 37 and 166 ppm in the spectra. The signals at 134, 136 and 178 ppm, corresponding to the aromatic and carboxylic carbon atoms of trimesate, were preserved regardless of the duration of the activation procedure, indicating the integrity of the linker molecules in the framework. Broadening of the signals, which became more apparent in longer activation procedures, can be attributed to local disorder and symmetry losses in the crystal structure.

The structural changes induced by the activation procedure were studied by monitoring the crystallinity, texture and particle morphology with powder X-ray diffraction (PXRD), nitrogen physisorption and scanning electron microscopy, respectively. X-ray diffractograms recorded before and after activation (Fig. S4†) show a decrease in crystallinity of the material. This is most likely due to the decomposition of the surface-bound nitrate anions, which induces stress in the parent framework; relaxation of the material will result in a loss of long range order and crystallinity. This observation is supported by the periodic PBE-D3 optimization, indicating a volume expansion of 4% in the case of a unit cell containing a defect site (see ESI†). However, both for the Ba- and Sr-based materials, major reflections at low angles can still be very clearly observed. This is in good agreement with the peak widening observed in the solid state NMR measurements of the activated samples. Relaxation of the materials, however, does not result in the complete deterioration of the material. Nitrogen physisorption measurements show a good retention of the microporosity upon activation at 320 °C for $Sr_2(BTC)(NO_3)$ (Fig. S5†), with an increase in BET surface area from 560 m^2 g^{-1} to 680 m^2 g^{-1}. Electron micrographs (Fig. S6†) indicate that there is a good retention of the particle morphology. Locally, signs of cracking and flaking of the material can be observed. This may further improve the catalytic activity of the material, as it shortens the diffusion pathways for the reactant molecules, which run lengthwise through the particles.

When combining the information gathered from various physicochemical techniques, the increased activity of $Ba_2(BTC)(NO_3)$ and $Sr_2(BTC)(NO_3)$ upon activation at high temperatures can be linked to the selective decomposition of a particular type of anion, *viz.* the structural nitrate anions. These nitrate ions line the pore walls and are important for the overall charge balance within the material (Fig. 1, bottom). As these anions are lost, charge neutrality can only be maintained by O^{2-} ions, which are introduced in the structure by the decomposition of nitrate (Scheme 2). Hence, the MOF with the structural formula $Ba_2(BTC)(NO_3)(DMF)_x$ is converted into an active catalyst with an approximate structural formula of $Ba_2(BTC)(NO_3)_{0.15}(O)_{0.425}$. As two nitrate anions are replaced by a single O^{2-} anion, multiple low-coordination metal sites are generated throughout the framework. These low-coordination metal ions, combined with the bridging O^{2-} anions, can thus be viewed as a new type of active site, explaining the overall catalytic activity of the materials. The Ba^{2+}–O^{2-}–Ba^{2+} motifs formed are highly reminiscent of the low-coordination sites found in alkaline earth oxides, but here nearly all of the Ba^{2+}–oxide units are available as active sites.

Additional evidence for the generation of such low-coordinated Ba or Sr sites comes from the observation of superoxide ions using electron paramagnetic resonance (EPR, Fig. 6). Prior to activation, no superoxide signals could be detected in the EPR spectra of the Sr- and Ba-MOFs. After activation at 320 °C, however, the new electron-rich active sites generated during activation, could interact with molecular oxygen, generating superoxide ions which are clearly visible in the spectra of both the Sr- and the Ba-MOFs. The g parameters from a fit are $g_{\|} = 2.087$ and $g_{\perp} = 2.005$ for activated $Ba_2(BTC)(NO_3)$; and $g_{\|} = 2.079$ and $g_{\perp} = 2.006$ for $Sr_2(BTC)(NO_3)$. Such values are highly characteristic of surface-bound superoxide anions.[26,27]

Finally, the basicity of the newly generated active site was compared with that of the original nitrate-rich material, using proton affinities (PAs) calculated *via* DFT-based simulations as a measure for the basicity.[28,29] Fig. 7 shows that the PA value of the Ba-MOF cluster increases substantially upon the transformation of the nitrate anions. In particular, when a defect site (–Ba–[*]–Ba–O–) is generated in the model, the computed PA value increases from 876 to 1153 kJ mol^{-1}. This effect is even more pronounced when a defect site is combined with a residual NO_3 unit: in that case, the computed PA value increases from 876 to 1233 kJ mol^{-1}. This increase in PA corresponds with an increase in basicity, and hence the theoretical analysis supports the observation that the introduction of a defect site results in an increased basic character. To gain insight into the strength of the newly generated basic sites, a comparison was made to the prototype basic material, cubic BaO. The PA values of a $(BaO)_{16}$ cluster show that the basicity of the newly generated active site is similar to that of the metal oxide cluster, which provides solid evidence for the basicity of the O^{2-} defect sites generated here.

Conclusions

In summary, the Sr- and Ba-MOFs $M_2(BTC)(NO_3)(DMF)$ were shown to be active base catalysts in different Knoevenagel condensation and Michael addition reactions. Their catalytic activity could be markedly increased *via* a vacuum pretreatment procedure at 320 °C. This was due to a loss of nitrate ions from the framework and the concomitant generation of new active sites consisting of low-coordination metal ions and O^{2-} anions. Theoretical analysis of the Ba-material shows that the basicity of the proposed Ba^{2+}–O^{2-}–Ba^{2+} motifs is close to that of the edge sites in BaO. This clearly illustrates that the discovery of new activation procedures is indispensable for the further development of MOFs as catalysts.

Acknowledgements

The authors are grateful to the Belgian Federal Government for support in the IAP project 07/05 Functional Supramolecular Systems, to KU Leuven for the Methusalem CASAS grant, and to FWO Vlaanderen for research project funding G.0453.09 and G.0486.12. P.V., T.D.B., M.V. and K.H. are grateful for a fellowship from FWO Vlaanderen. Funding was also obtained from the Research Board of Ghent University (BOF) and from the European Research Council under the European Community's Seventh Framework Programme (FP7(2007-2013) ERC grant agreement number 240483). MBJR acknowledges the European Research Council for financial support (ERC Starting Grant 307523) and the "Fonds voor Wetenschappelijk Onderzoek" (Grants G0197.11, G.0962.13). The authors would also like to thank Dirk Dom for performing the EPR measurements, Nico De Roo for performing the XPS measurements, Peter Salaets for performing the nitrate analysis and Kristin Coorevits for the elemental analysis.

Notes and references

1 J. R. Li, J. Sculley and H. C. Zhou, *Chem. Rev.*, 2012, **112**, 869–932.
2 A. Corma, H. García and F. X. Llabrés i Xamena, *Chem. Rev.*, 2010, **110**, 4606–4655.
3 P. Valvekens, F. Vermoortele and D. De Vos, *Catal. Sci. Technol.*, 2013, **3**, 1435–1445.
4 J. Gascon, U. Aktay, M. D. Hernandez-Alonso, G. P. M. van Klink and F. Kapteijn, *J. Catal.*, 2009, **261**, 75–87.
5 P. Kasinathan, Y. K. Seo, K. E. Shim, Y. K. Hwang, U. H. Lee, D. W. Hwang, D. Y. Hong, S. B. Halligudi and J. S. Chang, *Bull. Korean Chem. Soc.*, 2011, **32**, 2073–2075.
6 M. Savonnet, S. Aguado, U. Ravon, D. Bazer-Bachi, V. Lecocq, N. Bats, C. Pinel and D. Farrusseng, *Green Chem.*, 2009, **11**, 1729–1732.
7 Y. Tan, Z. Fu and J. Zhang, *Inorg. Chem. Commun.*, 2011, **14**, 1966–1970.
8 F. X. Llabrés i Xamena, F. G. Cirujano and A. Corma, *Microporous Mesoporous Mater.*, 2012, **157**, 112–117.
9 U. P. N. Tran, K. K. A. Le and N. T. S. Phan, *ACS Catal.*, 2011, **1**, 120–127.
10 C. Chizallet, S. Lazare, D. Bazer-Bachi, F. Bonnier, V. Lecocq, E. Soyer, A. A. Quoineaud and N. Bats, *J. Am. Chem. Soc.*, 2010, **132**, 12365–12377.
11 L. T. L. Nguyen, K. K. A. Le, H. X. Truong and N. T. S. Phan, *Catal. Sci. Technol.*, 2012, **2**, 521–528.
12 T. Maity, D. Saha, S. Das and S. Koner, *Eur. J. Inorg. Chem.*, 2012, **2012**, 4914–4920.
13 H. Hattori, *Chem. Rev.*, 1995, **95**, 537–558.
14 K. Tanabe and W. F. Hölderich, *Appl. Catal., A*, 1999, **181**, 399–434.
15 S. Coluccia, A. Barton and A. J. Tench, *J. Chem. Soc., Faraday Trans. 1*, 1981, **77**, 2203–2207.
16 S. Coluccia, A. J. Tench and R. L. Segall, *J. Chem. Soc., Faraday Trans. 1*, 1979, **75**, 1769–1779.
17 M. L. Foo, S. Horike, Y. Inubushi and S. Kitagawa, *Angew. Chem., Int. Ed.*, 2012, **51**, 6107–6111.
18 D. W. Lee, V. Jo and K. M. Ok, *Cryst. Growth Des.*, 2011, **11**, 2698–2701.
19 A. K. Cheetham, C. N. R. Rao and R. K. Feller, *Chem. Commun.*, 2006, 4780–4795.
20 K. Tanabe and K. Saito, *J. Catal.*, 1974, **35**, 247–255.
21 S. Bhaduri and D. Mukesh, *Homogeneous Catalysis: Mechanisms and Industrial Applications*, John Wiley & Sons, Inc., 2002.

22 M. B. J. Roeffaers, G. De Cremer, J. Libeert, R. Ameloot, P. Dedecker, A.-J. Bons, M. Bueckins, J. A. Martens, B. F. Sels, D. E. De Vos and J. Hofkens, *Angew. Chem.,Int. Ed.*, 2009, **48**, 9285–9289.
23 SDBSWeb: http://sdbs.riodb.aist.go.jp, National Institute of Advanced Industrial Science and Technology, 15 October 2013.
24 W. S. Epling, L. E. Campbell, A. Yezerets, N. W. Currier and J. E. Parks, *Catal. Rev.*, 2004, **46**, 163–245.
25 Y. S. Sayi, C. S. Yadav, P. S. Shankaran, G. C. Chhapru, K. L. Ramakumar and V. Venugopal, *Int. J. Mass Spectrom.*, 2002, **214**, 375–381.
26 M. Chiesa, E. Giamello and M. Che, *Chem. Rev.*, 2010, **110**, 1320–1347.
27 M. Anpo, M. Che, B. Fubini, E. Garrone, E. Giamello and M. Paganini, *Top. Catal.*, 1999, **8**, 189–198.
28 R. Cortese and D. Duca, *Phys. Chem. Chem. Phys.*, 2011, **13**, 15995–16004.
29 P. Valvekens, M. Vandichel, M. Waroquier, V. Van Speybroeck and D. De Vos, *J. Catal.*, 2014, **317**, 1–10.

